Short-wave infrared signature and detection of aicraft in flight based on space-borne hyperspectral imagery

Yueming Wang (王跃明), Feng Xie (谢 峰), and Jianyu Wang (王建宇)*

Key Laboratory of Space Active Opto-ElectronicsTechnology, Shanghai Institute of Technical Physics, Chinese Academy of Sciences, Shanghai 200083, China

**Corresponding author: jywang@mail.sitp.ac.cn*

Received May 26, 2016; accepted October 28, 2016; posted online December 9, 2016

Infrared signatures of aircraft are the basis for detection and monitoring. In past years, most of the studies focused on the aircraft's infrared signature in the mid-wave spectral region and long-wave spectral region for missile guidance or aircraft survivability studies. For the security of civil aviation, methods and instruments that can detect and monitor aircrafts from space are expected to be developed in the coming years. A short-wave infrared hyperspectral imager aboard the Tiangong-1 spacecraft acquired some civil aircraft's spectral data. The differences between the aircraft and the background in their spectral signatures are analyzed and discussed. Less absorption in the vapor absorption bands and a reflection spike is discovered at the 1.84 μm spectral band. The result shows that 1.84 μm and other vapor absorption bands can make contributions to aircraft detection in the daytime.

OCIS codes: 280.4788, 100.4145.
doi: 10.3788/COL201614.122801.

After Malaysia plane MH370 went missing, the detection and monitoring of aircraft became a hot topic in the world. For wide coverage, space-borne instruments are expected to play an important role. The signatures of aircraft are very complex because they are relevant to the type of aircraft, flight altitude, etc. Many investigations on aircraft's infrared signatures were conducted in the past decades. Most of them focused on the mid-wave infrared and long-wave infrared spectral regions for the application of missile guidance or countermeasures. Few of them paid attention to the signature in short-wave infrared (SWIR) spectral region. Generally speaking, higher resolutions can be achieved with same aperture diameters in the SWIR spectral region. To study the SWIR signature of aircraft, hyperspectral imaging technology is a useful tool. Hyperspectral imaging sensors are currently one of the most evolving and most promising technologies. Traditionally, hyperspectral imagery is used for earth science, mineral exploitation, etc. Classification utilizing hyperspectral data has been implemented extensively[1–10]. Indeed, hyperspectral imagery also plays an important role in acquiring a target's spectral signature.

The Tiangong-1 spacecraft was launched in 2011. The height of its orbit is about 400 km. A high-resolution SWIR hyperspectral imager is aboard in the spacecraft. It is a prismatic hyperspectral imager with high sensitivity in the SWIR bands. The main specifications are shown in Table 1. During its observations of the earth, two civil aircrafts were observed by accident.

They are both Boeing 737-sized aircrafts. One is southeast of Australia, and the other is in Malaysia. The pansharpened images are shown in Figs. 1 and 2, respectively.

Figures 1(a) and 2(a) are both pansharpened images (visible band). Figures 1(b) and 2(b) are zoomed-in images of Figs. 1(a) and 2(a) with aircraft at the center, respectively. Figures 1(c), 2(c), and 1(d) are the corresponding SWIR images and spectral curves.

Due to reflectance of solar irradiance, the two aircraft are both bright in the pansharpened images. The shapes of the aircrafts in the pansharpened image are clear. In Fig. 2(b), we can see a long contrail along the flight path of the aircraft. The contrail of aircraft comes from its exhaust plume. When the hot and wet exhaust plumes encountered cold air at high altitudes, the H_2O vapor of the exhaust plume transformed into ice particles, just like cirrus clouds. We also can infer that the aircraft in Fig. 1 was flying at a low altitude, so the contrail is not obvious. However, we cannot exclude a possibility that the aircraft

Table 1. Main Specifications of SWIR Hyperspectral Imager

Item	Specification
Spectral range (nm)	900–2500
Spectral interval (nm)	23.5
Band number	68
Ground sample distances (m)	20@400 km
Swath (km)	10@400 km
SNR (@SZA = 30°, ρ = 30%)	180@1700 nm; 120@2200 nm
Radiometric Calibration Accuracy	≤5%
Spectral Calibration Accuracy (nm)	≤2

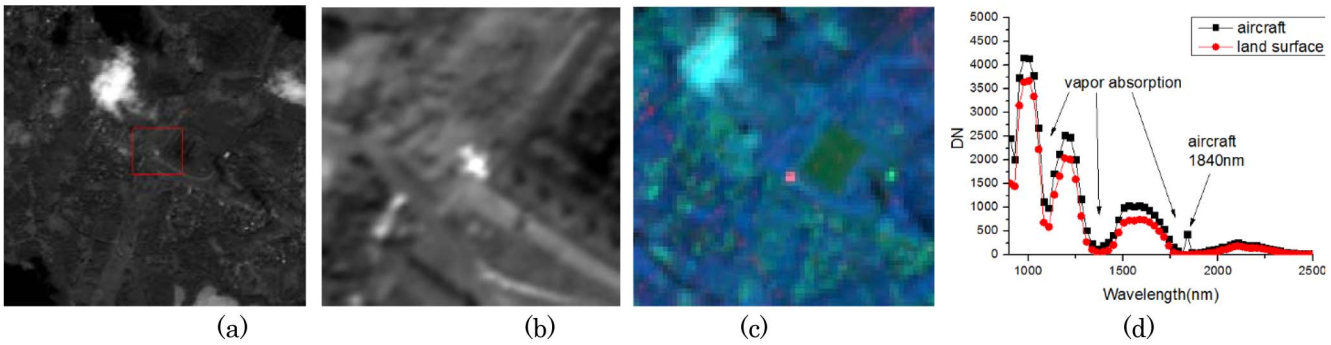

Fig. 1. Aircraft in 5 m pansharpened image in Malaysia. (a) Pansharpened image, (b) zoomed-in pansharpened image, (c) false RGB of SWIR, and (d) spectral curve of aircraft and clutter.

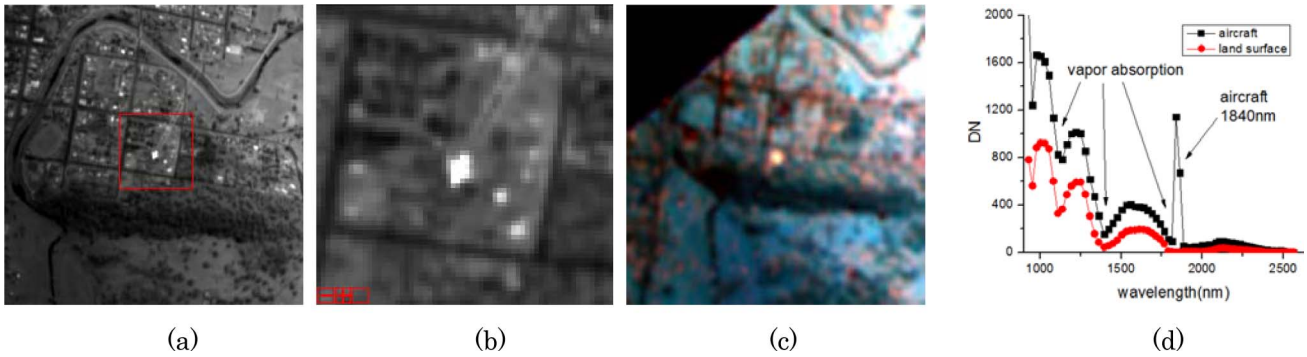

Fig. 2. Aircraft in 5 m pansharpened image in Australia. (a) Pansharpened image, (b) Zoomed-in pansharpened image, (c) false RGB of SWIR, and (d) spectral curve of aircraft and clutter.

was landing, so it discharged few exhaust plumes. The flight height of the two aircraft also can be deduced by the difference between the target and the background in the vapor absorption wavelength. In Fig. 1(d), the signal of the aircraft in the vapor absorption band is close to the background. In Fig. 2(d), it is obvious that the signal of the aircraft is higher than the clutter. The reason is that there is less vapor absorption at high altitudes than in the low atmosphere. The size of the ice particle is small enough that the contrail is almost transparent in the SWIR spectral region. Though the contrail is clear in Fig. 2(b), it is invisible in the image of the SWIR shown in Fig. 2(c).

On the basis of the signature analysis in the SWIR spectral region, we can discuss the capability of SWIR hyperspectral imagery for aircraft detection. The distinct advantage is the reflectance spike at the 1840 nm band. The signal can provide a high signal-to-clutter ratio (SCR) for target detection. Figure 3 shows the grayscale of the images at 1840 and 1700 nm. It is very difficult to find the aircraft in the image at 1700 nm because it is submerged in the clutter. A high SCR is shown in image of the 1840 nm band because the solar irradiance and solar reflection of clutter cannot penetrate the vapor absorption band. However, the aircraft is flying at a high altitude, so the solar irradiance is absorbed less than at lower altitudes. The instrument aboard the space-borne platform can detect the solar reflection of the aircraft body and its contrail.

The RX algorithm is a classic detector for hyperspectral anomaly detection. It is a basic multivariate anomaly detector[11]. It can be used for aircraft detection. Some experiments were conducted based on the RX algorithm. The RX algorithm is effective regardless of whether the target's signature is known or not. But if the signature of the object is clear, one can do a band selection to diminish the computation complexity.

Experiment 1: only two vapor absorption bands (1137 and 1395 nm) and 1840 nm bands are used in the calculation.

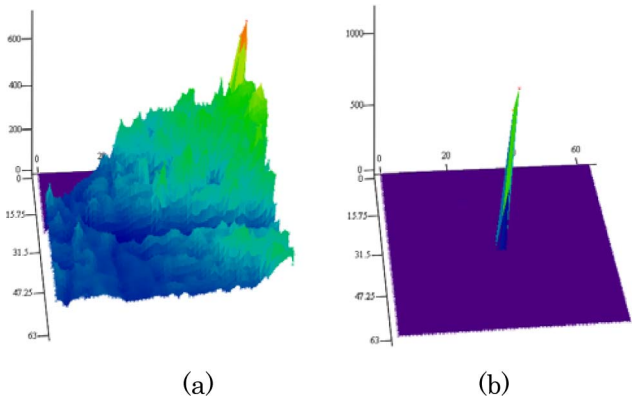

Fig. 3. Grayscale distributions of two band images. (a) 1700 nm band and (b) 1840 nm band.

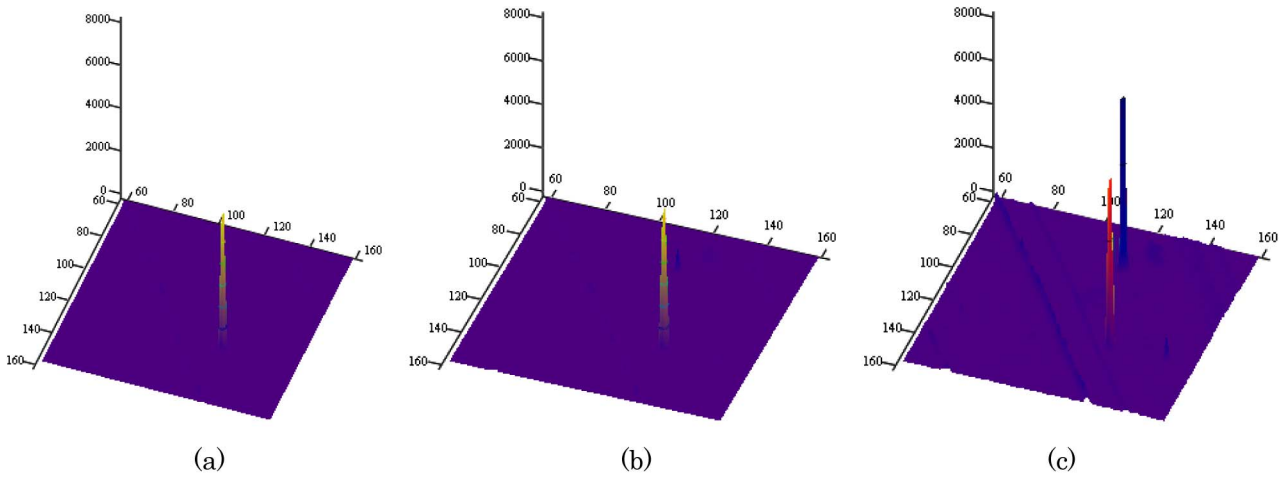

Fig. 4. RX anomaly detection result of data in Fig. 1. (a) Result of experiment 1, (b) result of experiment 2, and (c) result of experiment 3.

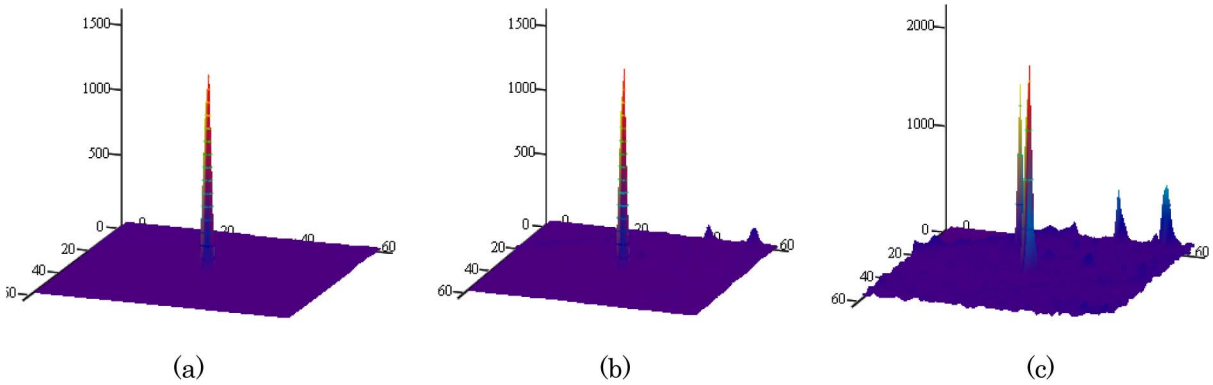

Fig. 5. RX anomaly detection result of data in Fig. 2. (a) Result of experiment 1, (b) result of experiment 2, and (c) result of experiment 3.

Experiment 2: four bands in atmospheric window are added in. They are 1029, 1221, 1612, and 2204 nm.

Experiment 3: all 68 bands are used in the calculation of the RX anomaly detection.

The Ground sample distances (GSDs) of the images used for experiments are the same, 20 m.

The RX anomaly detection results of the image data corresponding to Figs. 1 and 2 are shown in Figs. 4 and 5, respectively. In Figs. 4(a) and 5(a), the aircraft was shown clearly. That means a high SCR was achieved. In Figs. 4(b) and 5(b), some false alarms appeared. That means the SCR of the target decreases due to the introduced clutters in the atmospheric window bands. In Figs. 4(c) and 5(c), false targets emerged. That means more clutter was introduced as noise. The results indicate spectral signature bands play an important role in target detection. If the signature of the wanted target is definite, the RX anomaly detection algorithm can perform excellently. The bands that contain no signature will provide noise during the detection, so the false alarms will increase.

A large-area focal plane array and large aperture optics are the two main factors of the high cost of spaceborne instruments. If we can detect the aircraft with a lower-resolution instrument, that means a lower cost to manufacture the instruments. We also carried out an experiment to analyze the result of the RX anomaly detection when the pixels were binning. The spatial resolutions were 40 and 80 m. The data source is same as that shown in Fig. 2.

Comparing with Fig. 5(a), the SCR of the RX anomaly detection result also decreases with the decrease of the spatial resolution. The results of the target detected by

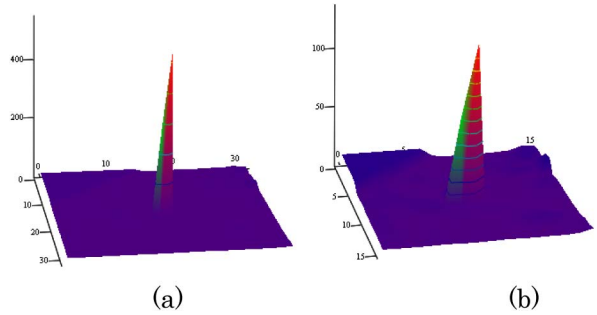

Fig. 6. Experiment result of lower spatial resolution. (a) 40 and (b) 80 m.

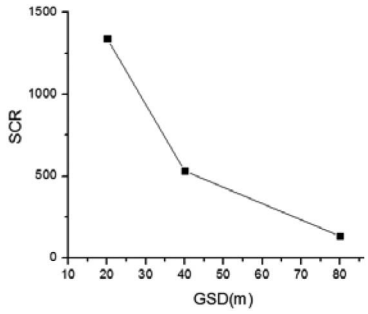

Fig. 7. Relationship between GSD and SCR.

the RX algorithm were 531 and 132, shown in Figs. 6(a) and 6(b), respectively. We drew a curve to describe the relation between the GSD and the SCR. With the increase of the GSD, the SCR decreased rapidly, as shown in Fig. 7.

In conclusion, the infrared spectral signature of an aircraft is clear when it flies at high altitudes. The signature mainly comes from less absorption in the vapor absorption bands. When the aircraft flies higher, the signature will be stronger. The RX anomaly detection algorithm is effective for the detection of aircraft based on SWIR hyperspectral imagery. Band selection plays a key role for maximizing the SCR of the detection. The spatial resolution is one important factor for detection probability. Trade-offs should be considered among all the factors, such as spatial resolution, cost, revisit period, etc.

This work was supported by the Innovation Funds from Chinese Academy of Sciences. The data used in this Letter were provided by the Tiangong-1 Service Platform for Promoting Space Utilization. We would also like to thank Chinese Manned Space Engineering, who funded the R&D of the high-resolution hyperspectral imager.

References

1. C. Liu, Z. Han, and T. Xie, Chin. Opt. Lett. **13**, 071701 (2015).
2. Q. Yang, Chin. Opt. Lett. **12**, 031201 (2014).
3. L. Xiu, C. Chen, Z. Zheng, L. Yin, Z. Yu, J. Huang, B. Huang, Q. Zhang, X. Xiu, and Y. Gao, Chin. Opt. Lett. **12**, 083002 (2014).
4. J. Karlholm and I. Renhorn, Appl. Opt. **41**, 6786 (2002).
5. S. Lefebvre, A. Roblin, and V. G. Durand, Reliab. Eng. Syst. Saf. **95**, 484 (2009).
6. Y. Ata and K. C. Nakiboglu, Opt. Commun. **283**, 3901 (2010).
7. W. A. Hovis, L. R. Blaine, and M. L. Forma, Appl. Opt. **9**, 561 (1970).
8. F. Liu, X. Shao, P. Han, B. Xiangli, and C. Yang, Opt. Eng. **53**, 094101 (2014).
9. H. Li, Y. Ma, K. Liang, and Y. Yu, Chin. Opt. Lett. **10**, 013001 (2012).
10. P. Du, W. Zhang, and J. Xia, Chin. Opt. Lett. **9**, 031002 (2011).
11. I. S. Reed and Y. Xiaoli, IEEE Trans. Acoust., Speech, Signal Process. **38**, 1760 (1990).